Symmetry-general least-squares extraction of elastic data for strained materials from *ab initio* calculations of stress

Yvon Le Page*
ICPET, National Research Council of Canada, Ottawa, Canada K1A 0R6

Paul Saxe†
Materials Design Incorporated, PMB No. 176, 825 College Boulevard, Suite 102, Oceanside, California 92057

(Received 18 July 2001; revised manuscript received 18 September 2001; published 13 February 2002)

A symmetry-general approach for the least-squares, therefore precise, extraction of elastic coefficients for strained materials is reported. It analyzes stresses calculated *ab initio* for properly selected strains. The problem, its implementation, and its solution strategy all differ radically from a previous energy-strain approach that we published last year, but the normal equations turn out to be amenable to the same constrainment scheme that makes both approaches symmetry general. The symmetry considerations governing the automated selection of appropriately strained models and their Cartesian systems are detailed. The extension to materials under general stress is discussed and implemented. VASP was used for *ab initio* calculation of stresses. A comprehensive range of examples includes a triclinic material (kyanite) and simple materials with a range of symmetries at zero pressure, MgO under hydrostatic pressure, Ti_4As_3 under [001] uniaxial strain, and Si under [001] uniaxial stress. The MgO case agrees with recent experimental work including elastic coefficients as well as their first and second derivatives. The curves of elastic coefficients for Si show a gradual increase in the 33 compliance coefficient, leading to a collapse of the material at −11.7 GPa, compared with −12.0 GPa experimentally. Interpretation of results for Be using two approximations [local density (LDA), generalized gradient (GGA)], two approaches (stress strain and energy strain), two potential types (projector augmented wave and ultrasoft), and two quantum engines (VASP and ORESTES) expose the utmost importance of the cell data used for the elastic calculations and the lesser importance of the other factors. For stiffness at relaxed cell data, differences are shown to originate mostly in the considerable overestimation of the residual compressive stresses at x-ray cell data by LDA, resulting in a smaller relaxed cell, thus larger values for diagonal stiffness coefficients. The symmetry generality of the approach described here enabled the creation of a robust user interface going seamlessly from the database search to the printout of the elastic coefficients. With it, even nonspecialist users can reliably produce technologically relevant results like those discussed here in a simple point-and-click fashion from corresponding entries in the CRYSTMET® and ICSD® structure databases, i.e., for all pure-phase nonorganic materials with known crystal structure. The case of Ti_4As_3 exposes, on a first cluster of properties, stiffness, compliance, and the isotropic properties that can be derived from them, the current reality of mining crystal structure databases with *ab initio* software for technological properties that were never measured before. Further developments in that direction are currently underway.

DOI: 10.1103/PhysRevB.65.104104 PACS number(s): 61.50.Ah, 62.20.Dc, 03.67.Lx, 61.68.+n

I. INTRODUCTION

There are two major ways of extracting elastic data through *ab initio* modeling of materials from their known crystal structures: an approach based on the analysis of the total energies of properly strained states of the material, and an approach based on the analysis of changes in calculated stress values resulting from changes in the strain. This ''stress-strain'' approach originates from the 1983 paper by Nielsen and Martin[1] about *ab initio* calculation of stress and its application to calculation of second-, third-, and fourth-order elastic constants. Additional developments and applications have since appeared in a comprehensive range of physics, materials, geophysics, and mineralogy journals. We only quote a few of them.[2–11]

In a previous publication,[12] we reported the improvement and automation of the energy-based approach. The present study develops the concepts and methods required to implement similar features, but with stress calculations. Differences mostly stem from the fact that energy is a scalar quantity while stress is a rank-II tensor. Advantages of the truly linear formulation of the stress-based problem are also exploited here to extend the method to the extraction of precise elastic data under given initial stress or strain, including large strains outside the harmonic regime around the equilibrium structure. One of the practical results of the present study is an automated tool operating seamlessly on entries for pure phases in the well-known crystal structure databases CRYSTMET (Ref. 13) and ICSD.[14] This tool, which is part of the MEDEA framework[15] and exploits the stress calculation in the VASP (Ref. 16) *ab initio* engine, produces their stiffness coefficients together with a number of related thermomechanical properties that are directly obtainable from them. We have tested the present method using this tool on a range of problems.

The text and equations below use the analytically simpler viewpoint that stress is produced when strain is applied to a relaxed material. Only Sec. III involves the conceptually opposite but physically equivalent viewpoint that materials strain under applied stress. Also, where we indicate ''strain''

in the absence of a clear context, we mean a small strain in addition to an initial strain. That initial strain is general and not restricted to isotropic deformations. For clarity, large applied strains are referred to as ''initial strain,'' ''total strain,'' etc. in all cases.

II. LEAST-SQUARES EXTRACTION OF ELASTIC COEFFICIENTS

A. The triclinic case

Using the matrix notation for elasticity, the well-known relationship

$$\sigma_i = \mathrm{sum}_{j=1,6} C_{ij}\varepsilon_j \tag{1}$$

describes the small stress components σ_i $(i=1,6)$ caused by application of a small strain ε with components ε_j $(j=1,6)$ to a relaxed crystalline compound. In this equation, C_{ij} are the elastic coefficients of the relaxed material. We spell out ''sum'' in Eq. (1) instead of the usual ''Σ'' symbol in order to avoid confusion with large stresses that will be designated ''Σ'' below. When rewritten in matrix form $\boldsymbol{\sigma}=\mathbf{C}\boldsymbol{\varepsilon}$, Eq. (1) then constitutes a linear system of six equations with six variables ε_j involving the 21 unknowns C_{ij}.

We do not wish to restrict ourselves to the elastic coefficients of the relaxed material, but also to model the elastic coefficients of the material under a known initial strain **E**. That initial strain, which could be large, causes a corresponding stress $\Sigma(\mathbf{E})$ that can be computed using appropriate *ab initio* modeling software, irrespective of whether **E** is within the harmonic range of the relaxed material or not. Total strains around value **E** can then be written $\mathbf{E}+\mathbf{e}$, with **e** small. Under those conditions, the linearity of the small stress changes **s** due to small strain changes **e** can be written

$$\Sigma(\mathbf{E}+\mathbf{e}) = \Sigma(\mathbf{E}) + \mathbf{s} = \Sigma(\mathbf{E}) + \mathbf{C}(\mathbf{E})\mathbf{e}. \tag{2}$$

Equation (2) is again linear and relates the stress change **s** and the strain change **e**, both small, through the elastic coefficients $\mathbf{C}(\mathbf{E})$ of the material under the large strain **E**.

The problem to be solved is to extract the constant values $\Sigma(\mathbf{E})$ and $\mathbf{C}(\mathbf{E})$ from a number of appropriately selected sample values $\Sigma(\mathbf{E}+\mathbf{e})$ calculated through *ab initio* modeling. When written as in Eq. (2), this problem is linear with 27 variables, namely, the six components of the initial stress $\Sigma(\mathbf{E})$ and the 21 independent coefficients $\mathbf{C}(\mathbf{E})$. It is then amenable to a least-squares solution, similar to that developed in Ref. 12.

1. Selection of the experimental data in the triclinic case

Triclinic refers here to the symmetry of the material under the initial strain **E**, which is not necessarily the symmetry of the unstrained material. The problem is simplified with respect to the energy-based approach by the fact that a stress calculation leads here to six ''experimental'' values per simulation, instead of one. It can be appreciated from Eq. (2) that one can then extract a whole row of the stiffness matrix $\mathbf{C}(\mathbf{E})$ through calculation of the stress change caused by a change in a single strain component. The stresses resulting from the seven total applied strains **E**, $\mathbf{E}+e_1$, $\mathbf{E}+e_2$,..., $\mathbf{E}+e_6$ are calculated. Row 1 of the stiffness matrix is extracted from the stress differences between the $\mathbf{E}+e_1$ and **E** simulations using Eq. (2), and row 2 from the stress differences between $\mathbf{E}+e_2$ and **E** etc. The six initial stresses $\Sigma(\mathbf{E})$ are the stresses calculated for **E**. As there are only 27 numbers extracted, six at a time during this procedure, one may wonder if they could be extracted from six or even five more adequately selected strains. It seems that this is not the case, and that fewer than seven simulations would not allow extraction of those quantities in the triclinic case, but we have no formal proof for this point.

B. Least squares and extension to nontriclinic crystals

The above simple-minded triclinic procedure is amenable to a symmetry-general least-squares scheme for the extraction of the independent coefficients like those detailed in Ref. 12, with analogies, but also with deep differences. There are differences in the layout of the problem, the refined variables because stress is refined instead of strain, the selection of appropriate strained states, and the solution strategy. The system of normal equations is accordingly derived in an entirely different way. The redundant system of equations to be solved by least squares was highly nonlinear for energy strain in Ref. 12. For stress strain, the system is linear, therefore the derivation of normal equations is not detailed here. It is remarkable that, in spite of such deep algebraic differences at the level of the redundant equations to be solved, the systems of normal equations derived from them can then be processed and resolved in conceptually parallel ways because *ab initio* stresses also obey the point-group symmetry of the strained crystal.

In a few words, an initial singular system involving 27 variables, some of them constrained, is built with properly selected ''experimental'' data. This system transforms into a regular system when it is expressed in terms of just the independent elastic coefficients through implementation of the constraints by corresponding rank reduction of the 27×27 matrix of normal equations. As the symmetry of an initially strained model might differ from that of the unstrained material, the symmetry constraints applying to $\mathbf{C}(\mathbf{E})$ might then differ from those applying to the elastic coefficients $\mathbf{C}(\mathbf{0})$ of the relaxed material.

The solution strategy also has to be different. As all terms involving initial strains were zero for zero values of the elastic coefficients in the energy-strain scheme,[12] the refinement had to be performed in two steps. In a first step, the elastic coefficients were refined with zero initial strains. Then, all variables were included in a second step which required several cycles to converge to numerical accuracy. Oppositely, the stress-strain problem is fully linear and first converges to numerical accuracy in a single cycle with unit weights and calculation of chi square. The equal weights are then adjusted to give the expected unit value of chi square. A second cycle is then performed to extract the standard deviations of the refined variables. True weighting of the individual observations can also be performed if desired.

TABLE I. Efficient strain schemes for various crystal systems in their IRE (Ref. 20) setting. The symmetry-general least-squares scheme presented in this paper has been tested to extract with no singularity the independent elastic coefficients and initial stresses from the *ab initio* computed stresses corresponding to the listed row of applied strains. The test was performed using a single magnitude of e for each crystal class in their respective crystal systems. For redundancy in the analyzed data, which is necessary to extract meaningful least-squares standard deviations, several magnitudes of e can be used. Those schemes are not unique. They may not preserve maximum crystal symmetry for each crystal class, or maximum Wyckoff symmetry of occupied sites for given crystal structures, but they are fairly efficient all-around schemes. We do not think that it is possible to obtain a nonsingular system of normal equations with fewer simulations than in the schemes below.

System	Strains						
Cubic	e_1,	$e_4+e_5+e_6$					
Hexagonal	e_1,	e_3,	e_4+e_5				
Tetragonal	e_1,	e_3+e_6,	e_4+e_5				
Orthorhombic	e_1,	e_2,	e_3,	$e_4+e_5+e_6$			
b-unique Monoclinic	e_1,	e_2,	e_3+e_6,	e_4,	e_5		
Triclinic	0,	e_1,	e_2,	e_3,	e_4,	e_5,	e_6

Proper selection of the experimental data for nontriclinic problems

The following strategy, which provides ample data while usually retaining symmetry in the distorted model, can be easily shown to lead to a nonsingular system of normal equations. We select a strain magnitude e and then generate in turn the seven above single-strain *ab initio* jobs $\mathbf{E}$, $\mathbf{E}+e_1$, $\mathbf{E}+e_2$, etc., eliminating the jobs with strains that are symmetry related to previously generated strains because they would produce numerically equivalent symmetry-related stresses. Practically, for cubic symmetry under initial strain, the total strains $\mathbf{E}$, $\mathbf{E}+e_1$, and $\mathbf{E}+e_4$ only are retained. For tetragonal symmetry, the coefficients are extracted from jobs implementing separately the five total strains $\mathbf{E}$, $\mathbf{E}+e_1$, $\mathbf{E}+e_3$, $\mathbf{E}+e_4$, and $\mathbf{E}+e_6$.

The justification for the above scheme is that, where an additional strain e_k was not implemented because a symmetry operation of the strained material would transform it into the previously generated strain e_j, we would also be able to transform the previously computed stress corresponding to e_j with the point-group symmetry operation relating the two strains. This would give the stress corresponding to strain e_k through straightforward tensor transformation of stresses under a rotation of the reference system rather than through a lengthy *ab initio* simulation. All the stresses corresponding to the seven triclinic strains would be recovered in this way. This process, which only implements point-group symmetry, then allows calculation of all 21 C_{ij} coefficients for the symmetric material, irrespective of any constraint possibly relating them. It follows that the starting data was therefore sufficient to solve for the independent coefficients. After rank reduction, a process that essentially migrates the stress data without loss of numerical information for the purpose of expressing the problem in terms of just the independent variables, the system of normal equations will then not be singular.

The same reasoning can be used to establish that data sufficient to extract analytically the independent stiffness coefficients and initial strain from the computed stress values by any other method would also be sufficient if processed through the above constrained least-squares procedure. For example, Table I lists one such sufficient set of strains for all point groups in each crystal system. Some of those strain combinations have been used before (e.g., Ref. 10 clearly used the same orthorhombic combination of strains), but some of them may be new. We have checked numerically that, with use of the strains in Table I implemented with a single strain magnitude, the constrained least-squares matrix is nonsingular for each point group in each crystal system. Singularity not being a matter of magnitude, use of this scheme at several strain magnitudes could then constitute a sensible way to collect appropriate stress data to extract least-squares elastic coefficients with just the desired degree of redundancy required to get standard deviations with adequate precision.

III. DUALITY OF THE FORMULATIONS IN TERMS OF STRESS AND STRAIN

Equation (1) translates the viewpoint that stress in a material is the result of applied strain. The corresponding physical property relating stress and strain is called the stiffness $\mathbf{C}$. In *ab initio* calculations, strain changes transform directly into changes in the input cell data, with no approximation involved. The corresponding stress is the result of the *ab initio* calculation. The opposite viewpoint that strain appears as a result of applied stress can be written

$$\varepsilon_i = \mathrm{sum}_{j=1,6}\, S_{ij}\sigma_j . \tag{3}$$

The corresponding physical property expressed by the 6×6 $\mathbf{S}$ matrix relating stress and strain is called the compliance. It follows from Eqs. (1) and (3) that $\mathbf{S}=\mathbf{C}^{-1}$. Implementation of this viewpoint does not lead to a major reformulation, but may involve some degree of recycling as illustrated in Fig. 1. In simulations aimed at establishing the conformation of the material under a known stress, small stress steps are successively applied to the material. These stress steps must be sufficiently small for the strain calculated with Eq. (3) to be

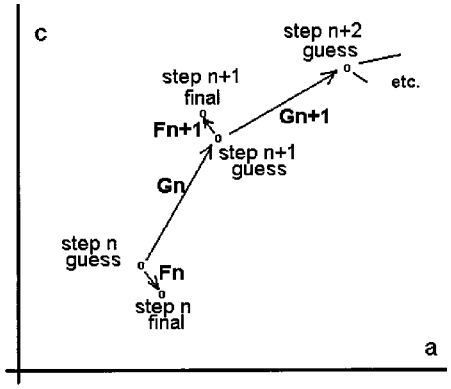

FIG. 1. Implementation of stress steps in two cycles in the simple case where two cell parameters, *a* and *c*, are adjustable. In the general case, six cell parameters are adjustable. At each step *n*, $n+1$, etc, an *ab initio* stress and compliance calculation is performed. This stress and compliance data allow calculation of both a small strain correction $\mathbf{F}_n$, $\mathbf{F}_{n+1}$, etc. for the current guess and a large strain step $\mathbf{G}_n$, $\mathbf{G}_{n+1}$, etc. giving the next guess. The small corrections $\mathbf{F}_n$ etc. being within the linear range of elasticity at step *n*, the corresponding cell data is then accurate.

approximately correct, say within a few percent. This strain is applied to cell data $\mathbf{D}_{n-1}$, giving cell data $\mathbf{D}_n$. A stress, stiffness, and compliance recalculation is then performed for cell data $\mathbf{D}_n$. Those stress and compliance data calculated for $\mathbf{D}_n$ in turn allow calculation of two strains $\mathbf{G}_n$ and $\mathbf{F}_n$.

$\mathbf{F}_n$ is a very small strain correction for the difference between the calculated stress and the desired stress for step *n*. That difference is usually so small that elastic linearity is now accurately obeyed. The cell data corresponding to application of $\mathbf{F}_n$ to the current cell data will then accurately match the desired stress.

The strain $\mathbf{G}_n$ corresponds to the application of the next stress step, taking into account the now known small strain offset $\mathbf{F}_n$. A stress calculation after application of $\mathbf{G}_n$ will again give a stress value differing from the desired value by a tiny difference, giving in turn the tiny cell data correction $\mathbf{F}_{n+1}$ and the cell data adjustment $\mathbf{G}_{n+1}$ for a further stress step etc.

This way of proceeding does not require inclusion of a general stress in the expression of the Hamiltonian, but just the capability of computing the stress and the compliance for a given cell configuration. Convergence of this procedure is so fast that we use it even where the stress is a simple hydrostatic pressure. This is partly because MEDEA retains in this way the ability to drive for the same purpose quantum codes that do not include the cell optimization under pressure among their features. It is also partly because we feel that this way of proceeding might be computationally efficient in view of the fact that no *ab initio* cell optimization in the quantum code is involved. Elastic relaxation based on the result of the *ab initio* compliance calculation for the input cell data is instead applied later. The two methods are probably computationally fairly equivalent with hydrostatic pressure, but the present approach also allows efficient elastic calculations under a general stress as well, with an example developed in Secs. V E and VI E below.

IV. "EXPERIMENTAL" PRECAUTIONS

Several precautions must be taken in order to ensure that changes in calculated stress values between simulations originate in a model change and not mostly in a different positioning of integration sampling points with respect to the quantity being integrated. For energy purposes,[12] it was sufficient to use the same primitive vectors, with the same origin with respect to the crystal structure, and divide them in a consistent way throughout the simulations. Energy being a scalar quantity and therefore independent of the selected axial system, each simulation could then be referred to the Institute of Radio Engineers[20] (IRE) system that was corresponding to its symmetry. With stress analysis, the orientation of the Cartesian system as well must be retained throughout the simulations of the various strained models with the various subgroup symmetries. The corresponding manipulation of the structure models is straightforward.

V. EXAMPLES OF ACTUAL DERIVATION OF ELASTIC COEFFICIENTS

As described in the previous section, the present method has the capability of deriving elastic data under a general strain or stress. Although this is of significant technological interest, we failed to locate experimental elastic data under stress other than hydrostatic pressure, but we found a phase-transformation report for Si under uniaxial [001] stress.[17] Such calculated numbers would nevertheless be useful towards, e.g., studies involving mechanical properties of epitaxial layers of materials with poor cell data match, or with different thermal-expansion coefficients.

A. Triclinic example: kyanite

The only tractable example we could find where the elastic coefficients of a material had either been computed or measured is that of kyanite, a triclinic polymorph of Al_2SiO_5. The elastic coefficients were recently computed by two methods by Winkler, Hytha, Warren, Milman, Gale, and Schreuer.[18] Like them, we used the cell and fractional coordinate data from Winter and Ghose[19] as starting points. Provided that right-hand reference systems are used throughout as they should, the somewhat suspicious 90° triclinic α angle does not lead to a setting ambiguity of the atomic structure with respect to the lattice or of the lattice with respect to the IRE (Ref. 20) axes.

The simulations were performed with the following parameters: Generalized-gradient approximation (GGA) projector augmented wave (PAW) potentials,[21] relaxation convergence of 10^{-4} eV, electronic convergence of 10^{-5} eV, conjugate gradient optimization of the wave functions, reciprocal-space projection, a $3\times3\times3$ *k* mesh for the reciprocal-space integration with a Monkhorst-Pack scheme,[22] and the tetrahedron method with Blöchl (Ref. 21) corrections for the energy. We used the triclinic scheme in Table I, with strain values $+0.01$ and -0.01, leading to the 13 simulations that are reported in Table II together with resulting stress data. That stress data is a simple rearrangement with sign change of the cell forces that are printed by

TABLE II. Stress data for kyanite. The first six integers on each odd row are the applied strains in percent. The next six numbers on the same line are the forces on the cell as produced by VASP, transformed into stress components in kilobars and rearranged in the familiar order 1–6. Corresponding least-squares or recalculated values are shown with standard errors on the last printed digit inside parentheses.

0 0 0 0 0 0	8.44	4.87	6.28	1.95	0.34	−0.18
Least squares	8.36(9)	4.63(9)	5.88(9)	2.07(9)	0.23(9)	0.26(9)
1 0 0 0 0 0	45.27	15.30	12.82	2.08	0.42	−0.54
Recalculation	45.98	15.40	12.90	2.10	0.51	−0.55
−1 0 0 0 0 0	−29.99	−6.03	−1.11	2.01	−0.12	0.11
Recalculation	−29.27	−6.15	−1.13	2.04	−0.45	0.41
0 1 0 0 0 0	19.31	39.81	17.17	0.13	0.18	−0.02
Recalculation	19.13	40.29	17.12	0.24	0.17	0.09
0 −1 0 0 0 0	−2.46	−31.51	−5.60	4.22	0.36	−0.69
Recalculation	−2.42	−31.03	−5.35	4.12	0.29	−0.60
0 0 1 0 0 0	15.36	15.62	41.91	−0.29	0.50	−0.13
Recalculation	15.37	15.86	42.84	−0.16	0.55	−0.18
0 0 −1 0 0 0	1.23	−6.55	−32.01	4.33	−0.17	−0.46
Recalculation	1.34	−6.60	−31.08	4.30	−0.08	−0.49
0 0 0 1 0 0	8.55	2.83	4.29	19.06	0.32	0.13
Recalculation	8.38	2.58	3.66	18.93	0.21	−0.05
0 0 0 1 0 0	8.50	6.93	8.58	−14.66	0.32	−0.39
Recalculation	8.33	6.68	8.11	−14.79	0.26	−0.47
0 0 0 0 1 0	8.72	4.50	6.26	1.97	9.15	−0.95
Recalculation	8.63	4.57	6.20	2.05	9.19	−0.93
0 0 0 0 1 0	8.15	4.56	5.67	2.07	−8.77	0.49
Recalculation	8.08	4.69	5.57	2.10	−8.73	0.42
0 0 0 0 0 1	8.50	5.27	6.42	2.19	−0.38	11.72
Recalculation	8.06	4.97	6.12	2.28	−0.44	11.81
0 0 0 0 0 1	9.04	4.57	5.80	1.87	0.87	−12.42
Recalculation	8.65	4.29	5.65	1.86	0.90	−12.33

VASP. Table III reports the least-squares values of the elastic coefficients while the corresponding initial stresses are found under the first line in Table II. As an indicator of precision, we quote the residual after refinement $R=\text{sum}|Sc-So|/\text{sum}|So|$, where *So* is an individual observed stress component and *Sc* is the corresponding component calculated by inserting the refined least-squares values of **C** and Σ in expression (2) above. The sums extend over all individual components, i.e., six values per simulation. The residual after refinement calculated in this way is 2.3%. The total time taken by the 13 simulations was 2 h short of 8 days. Those elastic calculations followed a careful optimization of the coordinate data, but not of the x-ray cell data.

B. No applied pressure

Tables IV–VI show the stiffness results for the same materials that were used in Ref. 12, but now obtained with VASP (Ref. 16) from calculated stress changes about the experimental x-ray cell data. In Ref. 12, the numbers were obtained with ORESTES,[23] from calculated energy changes about the relaxed configuration. In both cases though, the cell data reported are the relaxed cell data.

For the stiffness calculations, we used two strain magnitudes, 0.007 and 0.01, with both signs,[3] leading to a sufficient redundancy of the nonzero stress component data for least-squares processing. For cubic compounds, this means that we used the strains 0, $+/-e_1$, and $+e_4$ at two strain magnitudes, i.e., a total of seven simulations leading to refinement of four numbers with 11 independent observations of nonzero stress components. For hexagonal compounds, the strains were 0, $+/-e_1$, $+/-e_3$, and $+e_4$ at the two magnitudes indicated above, i.e., a total of 11 simulations, etc.

TABLE III. Extracted elastic coefficients (see Table II). Similar data from Ref. 26 are italicized.

376(2)	108(2)	70(2)	0(2)	3(2)	−3(2)
387(2)	*100(1)*	*46(1)*	*−3(1)*	*0(1)*	*−6(1)*
108(2)	357(2)	112(2)	−20(2)	−1(2)	3(2)
	355(2)	*122(1)*	*−22(2)*	*−3(1)*	*3(1)*
70(2)	112(2)	370(2)	−22(2)	3(2)	2(2)
		366(1)	*−30(2)*	*3(1)*	*0(2)*
0(2)	−20(2)	−22(2)	169(2)	0(2)	2(2)
			182(2)	*−2(2)*	*0(3)*
3(2)	−1(2)	3(2)	0(2)	90(2)	−7(2)
				80(1)	*−6(2)*
−3(2)	3(2)	2(2)	2(2)	−7(2)	121(2)
					132(1)

TABLE IV. Cubic system: three elements and a binary compound (experimental data from Ref. 39).

	C_{11}	C_{12}	C_{44}	
	(GPa)			a (Å)
C	1064	132	565	3.574 6 calculation, this study
	1079	124	578	3.566 91 experiment
	1013	174	603	3.513 3 calculation[a]
Al	106	57	28	4.042 3 calculation this study
	114	62	32	4.049 4 experiment
	120	61	34	3.991 2 calculation[a]
Cu	187	133	81	3.633 1 calculation, this study
	168	121	75	3.614 65 experiment
	214	155	99	3.559 5 calculation[a]
GaAs	118	59	55	5.731 5 calculation, this study
	119	53	60	5.653 3 experiment
	112	55	51	5.745 1 calculation[a]

[a]Reference 12.

The following VASP input or execution parameters were used: GGA PAW potentials,[21] relaxation convergence of 10^{-6} eV, electronic convergence of 10^{-7} eV, conjugate gradient optimization of the wave functions, reciprocal-space projection, a $15\times15\times15$ k mesh for the reciprocal-space integration with a Monkhorst-Pack scheme,[22] and the tetrahedron method with Blöchl (Ref. 21) corrections for the energy. The same simulation conditions were used throughout this manuscript, except where differences are noted.

C. Hydrostatic pressure applied

We chose MgO as a test example because it has been studied theoretically by, e.g., Karki *et al.*,[9] experimentally by Yoneda,[24] then more recently in the diamond-anvil cell by Sinogeikin and Bass,[25] as well as Zha, Mao, and Hemley[26] thus offering a good opportunity for comparisons. The theoretical study[9] mostly extends up to 150 GPa while the experimental pressure in Ref. 25 does not exceed 20 GPa because of the nonavailability of immersion media capable of transmitting higher hydrostatic pressures. However, additional experimental data by Duffy and Ahrens[27] extends up to 237 GPa. We accordingly scanned the range from 0 to 237 GPa, but with a greater density of data points in the 0–20-GPa range.

In this section, for the purpose of easy comparison with previous experimental and theoretical literature results, we use the geophysical convention that compressive stresses are positive. Among other things, this changes the orientation of the pressure axis with respect to the physical convention that compressive stresses are negative. Also, odd-order derivatives of the elastic coefficients in Table VII change sign un-

TABLE V. Hexagonal system. Two hcp elements and a rhombohedral compound. Five stress calculations are at each of two strain magnitudes, 0.7% and 1%. Residual 1.3% using a reciprocal space mesh of $23\times23\times23$. For Be, hcp there are five stress calculations at each of two strain magnitudes, 0.7% and 1%. Residual 0.8% using a reciprocal space mesh of $23\times23\times23$. Atomic positions for Al_2O_3 were optimized in the present study, while they were not in Ref. 12.

	C_{11}	C_{12}	C_{13}	C_{33}	C_{44}		
	(GPa)					a	c (Å)
Mg (hcp, $P6_3/mmc$)							
11 simulations	49	31	21	58	14	3.1906	5.1800 calculation, this study
Experiment[a]	59	26	21	61	17	3.2089	5.2101
27 differences	70	31	24	74	22	3.1354	5.0909 calculation[b]
Be, hcp							
11 simulations	290	23	12	364	162	2.2639	3.5663 calculation, this study
Experiment[c] (0 K extrapolation)	299	27	11	342	166	2.2826	3.5836
18 differences	336	81	21	443	181	2.1851	3.4710 calculation[b]

Al_2O_3, R-3c

	C_{11}	C_{12}	C_{13}	C_{14}	C_{33}	C_{44}		
	(GPa)						a	c (Å)
Calculation, this study	495	171	130	20	486	148	4.7642	12.994
Experiment[a]	500	162	111	−23	502	151	4.754	12.982
Calculation[b]	518	131	92	17	475	128	4.7040	12.706

[a]Reference 39.
[b]Reference 12.
[c]Reference 40.

TABLE VI. Tetragonal element. Six stress calculations are at each of two magnitudes, 0.7% and 1%. Residual 1.3% using a reciprocal space mesh of $15\times15\times15$.

	C_{11}	C_{12}	C_{13}	C_{33}	C_{44}	C_{66}		
			(GPa)				a	c (Å)
				In, $I4/mmm$				
Calculation, this study	55	44	41	46	4	12	3.3162	4.9002
Experiment[a]	45	40	41	45	7	12	3.2523	4.9461
24 differences[b]	71	36	46	58	11	17	3.0971	5.1905

[a]Reference 39.
[b]Reference 12.

der a change of convention, while even-order ones are unchanged. The physical convention is used in the rest of the manuscript.

The *ab initio* stress calculations totaled about two days of computing time on a 1.4-GHz Pentium 4. The present least-squares procedure analyzed the corresponding stress data in less than a second for each of the 20 data points.

With this data, we produced graphs of C_{ij}, K, and G vs hydrostatic pressure. They were so equivalent to those in Ref. 9 that they were not worth showing. We only show here Fig. 2 that reports the cubic cell volume for MgO vs hydrostatic pressure. The fit with experimental data[27–30] is excellent, quite possibly within experimental error. Additional ''low-pressure'' data from Ref. 26 and other experimental work quoted in, e.g., Ref. 25 would superimpose nicely with the data already plotted in Fig. 2.

A least-squares fit of the *ab initio* stiffness data points by a polynomial expression was performed for each stiffness coefficient. Values and derivatives at zero pressure of the various stiffness coefficients were then read off the coefficients of that polynomial fit. They are reported in Table VII together with experimental and theoretical literature data.

D. Uniaxial strain applied to Ti_4As_3

Application of a general strain, for example, a uniaxial strain, is straightforward. The components **L** of the lattice

TABLE VII. Present MgO results and comparison with previous work. The independent stiffness coefficients C_{ij}, Young's modulus K, the shear modulus G, and their first and second derivatives according to the present work and Refs. 9, 24–26. Note that the geophysical convention that compressive stresses are positive is used in this table and in Sec. V C and VI C, but not elsewhere.

Stiffness coefficients (GPa)	C_{11}	C_{12}	C_{14}	K	G
This work	303.7	97.2	148.2	166.0	130.2
Sinogeikin and Bass[a]	297.9	95.8	154.4	163.2	130.2
Yoneda[b]	297.8	95.1	155.8	162.7	
Zha, Mao, and Hemley[c]	297.0	95.2	155.7	162.5	130.4
Karki[d] *et al.*	291	91	139	159.4	126.8
First derivatives (no units)	C'_{11}	C'_{12}	C'_{14}	K'	G'
This work	8.91	1.59	0.99	4.03	2.06
Sinogeikin and Bass[a]	9.05	1.34	0.84	3.96	2.35
Yoneda[b]	8.75	1.90	1.30	4.1	
Zha, Mao, and Hemley[c]	9.7	0.82	1.09	3.99	2.85
Karki[d] *et al.*				4.28	2.18
Second derivatives (GPa^{-1})	C''_{11}	C''_{12}	C''_{14}	K''	G''
This work	−0.035	−0.011	−0.018	−0.019	−0.016
Sinogeikin and Bass[a]	−0.090	−0.002	0.006	−0.044	−0.040
Yoneda[b]	−0.034	−0.003	−0.082	−0.028	
Zha, Mao, and Hemley[c]	−0.126	+0.06	−0.009		−0.084
Karki[d] *et al.*				−0.027	−0.022

[a]Reference 25.
[b]Reference 24.
[c]Reference 26.
[d]Reference 9.

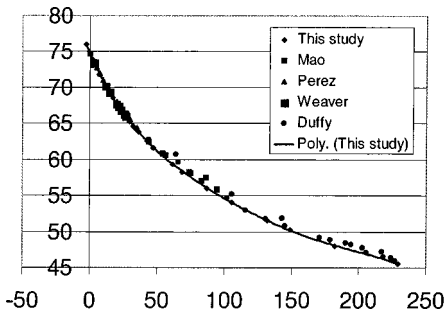

FIG. 2. Graph of cell volume in $Å^3$ vs hydrostatic pressure for MgO. The curve is a polynomial fit to the *ab initio* data points calculated for the present study. Experimental data points by Mao and Bell (Ref. 28), Perez-Albuerne and Drickamer (Ref. 29), Weaver, Takahashi, and Bassett (Ref. 30), and Duffy and Ahrens (Ref. 27) are also shown in the graph.

translations are worked out for the Cartesian system where the strain **E** has been defined. Application of the strain gives new components $\mathbf{L}'=(\mathbf{E}+\mathbf{I})\mathbf{L}$. The new lattice data is calculated from $\mathbf{L}'$ directly and with no approximation. We have, for example, performed in the above way the calculations corresponding to the [001] uniaxial compression of Ti_4As_3 up to 10 GPa with (001) clamped.

Ti_4As_3 seems to have only been prepared in powder form. Its Th_3P_4 structure type was established by Berger in 1977.[31] Table VIII echoes the CRYSTMET database entries for this material and for Th_3P_4. There are marked differences between the two compounds. They have quite different cell volumes [453 vs 640 $Å^3$] and the crystal-chemical roles played by cations and anions are opposite. Strictly speaking, Ti_4As_3 should then be assigned the anti-Th_3P_4 type when considered to be an inorganic compound. All this points to possible large differences in atom coordinates, although the *x* coordinate of Ti is the only free parameter in the unstrained state of this compound.

An *ab initio* optimization of cell and structure converged to $a=7.6779$ Å, Ti $x=0.0753$. The optimized cell edge is in perfect agreement with the experimental value of 7.6795(2) Å. This constitutes a solid support for the assignment of the Th_3P_4 type to Ti_4As_3 by Berger.[31] The refined *x* coordinate shows that Ti has moved by 0.107 away from the value $x=\frac{1}{12}$ that would place it at equal distance from two sets of (111) equilateral triangles of As neighbors with positions fixed by symmetry. On the contrary, from CRYSTMET entry AL4092, P seems to have that $x=\frac{1}{12}$ coordinate value within experimental error in Th_3P_4.

After the *ab initio* transformation of the cell and structure-type CRYSTMET entry AL4132 into a credible full crystal structure description as performed above, we then proceeded with *ab initio* computing of its elastic coefficients. In the unstrained state, Ti_4As_3 has only one refinable coordinate parameter, but under strain e_4, for example, the model becomes monoclinic with space group $C2$ and 20 adjustable atom coordinates. We get $C_{11}=273$, $C_{12}=71$, and $C_{44}=61$ GPa. Young's, shear, and bulk moduli for the isotropic material are first derived from them[32] as 138, 75, and 190 GPa. This in turn predicts the speed of sound for longitudinal and transverse waves to be, respectively, 6237 and 3496 m/s. From the mean sound velocity of 3791 m/s, a Debye temperature of 446 K is obtained,[32] leading to, e.g., a thermal-expansion coefficient of 11×10^{-6} K^{-1} at 300 K assuming a value of 2.0 for Grüneisen's coefficient. All those calculations are automatically performed in less than a second on the elastic coefficients refined by our software, with printout on the same sheet as *ab initio* stiffness and of course compliance.

We then proceed to uniaxial compressive straining of Ti_4As_3 along [001], i.e., shortening *c* while retaining fractional coordinates as well as the lengths of the *a* and *b* cell edges. The strained material therefore becomes tetragonal with six independent stiffness coefficients. In this section and in Sec. V E below, we used the same VASP parameters as in Sec. V B above except that we implemented here a $5\times5\times5$ *k* mesh. Results are reported in Fig. 3 for all six coefficients C_{11}, C_{12}, C_{13}, C_{33}, C_{44}, and C_{66}.

E. Uniaxial stress applied

Application of a general stress is slightly more difficult than application of a strain because that involves recycling.

TABLE VIII. CRYSTMET (Ref. 13) entries for Ti_4As_3 and Th_3P_4, reprinted with permission.

Entry	Formula	Structure type	Space group	Pearson symbol
AL4132[a]	Ti_4As_3	Th_3P_4	*I*-43*d* (220)	cI28
AL4092[b]	Th_3P_4	Th_3P_4	*I*-43*d* (220)	cI28

Cell dimensions

	a	*b* (Å)	*c*	*α*	*β* (°)	*γ*	Volume ($Å^3$)	*Z*
AL4143	7.6795(2)	7.6795(2)	7.6795(2)	90	90	90	452.90	4
AL4092	8.6170	8.6170	8.6170	90	90	90	639.84	4

Atom type	Wyckoff site	Site symmetry	Fractional coordinates			Uiso	Occupancy
P	16*c*	.3	0.083	0.083	0.083	0.50	1.0
Th	12*a*	−4	$\frac{3}{8}$	0	$\frac{1}{4}$	0.50	1.0

[a]Reference 31.

[b]K. Meisel, Z. Anorg. Allg. Chem. **240**, 300 (1939).

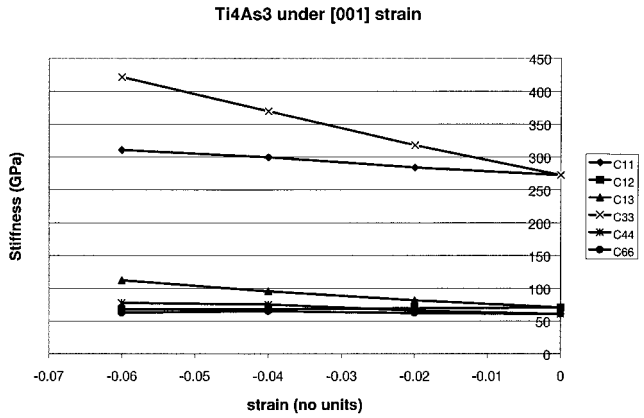

FIG. 3. Elastic coefficients of Ti_4As_3 under [001] uniaxial strain, i.e., clamped in (001).

In order to apply a uniaxial compressive stress along [001] to Si, meaning that Si can freely expand in the (001) plane, we followed the procedure outlined in Sec. III above. We used 2-GPa stress steps in order to calculate the strain steps $\mathbf{G}_n$. The subsequent strain corrections $\mathbf{F}_{n+1}$ turned out to correspond to a few hundredths of a GPa, giving cell data convergence to a high accuracy in two elastic calculations at each step. The compressed material expands along *X* and *Y* while it shrinks along *Z*, thus acquiring tetragonal symmetry, requiring the tetragonal elastic coefficients in Fig. 4 that are additional to the independent cubic coefficients. The MEDEA software[15] generates transparently those coefficients through automated handling of the corresponding symmetry aspects.

F. LDA vs GGA and energy strain vs stress strain in the case of beryllium

The discrepancy between the C_{12} values obtained by a LDA/energy-strain approach implemented with the ORESTES quantum engine and those obtained by a GGA/stress-strain approach with the VASP engine is very large and puzzling. Although there is little doubt as to which set of results agrees better with the experiment, we performed additional tests based on the beryllium results in Table V, with the purpose of exploring the noted differences in relaxed cell data between the various engines and approximations used.

In addition to echoing the Be results of Table V, Table IX reports additional elastic calculations for Be, all computed with the same execution parameters except those noted. The conditions adjusted were the cell data and the type of approximation and are detailed in Sec. VI F.

VI. DISCUSSION

It seems that one of the main advantages of the stress-based approach is that, as seen in Eqs. (1) or (2), and as previously pointed out by Wentzcovitch, Karki, Karato, and Da Silva[3] the derived stress change is a first-order function of the small applied strains. Oppositely, the derived energy change is a second-order function of the applied strain change. As a consequence, the stress-based approach can implement small strains and still give fairly precise stress changes where the corresponding energy changes would be so small that they would necessarily be imprecise.

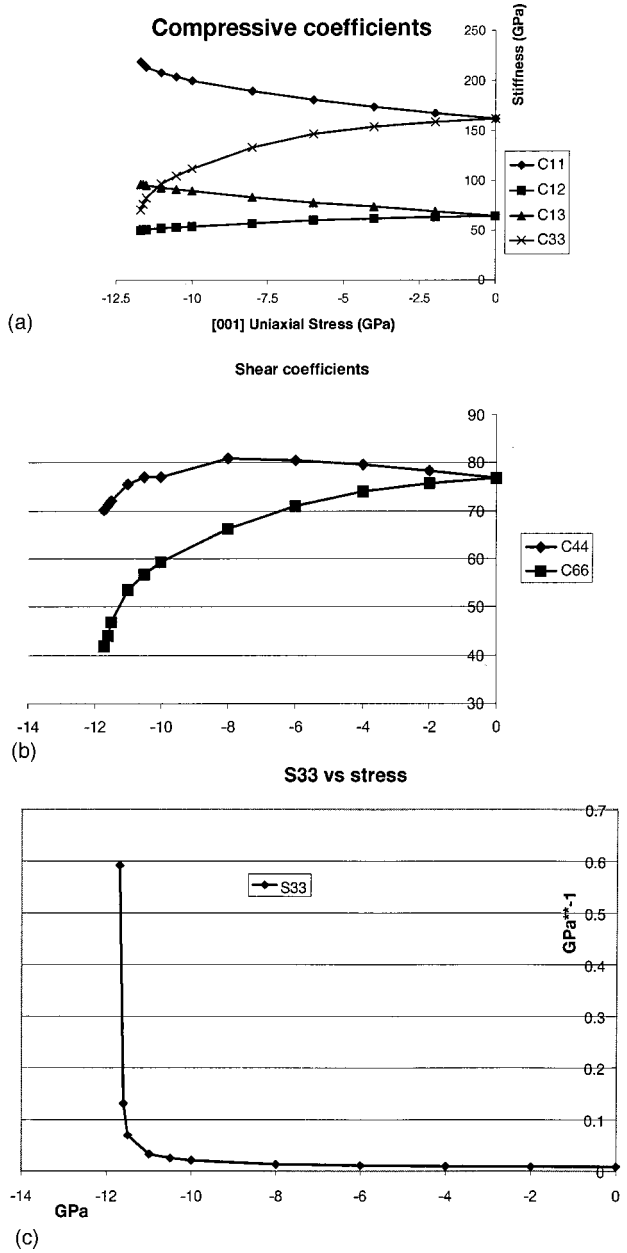

FIG. 4. (a) and (b) Elastic coefficients for Si uniaxially stressed along [001]. The material becomes tetragonal when subjected to this kind of stress. It hardens along [100] and softens considerably along [001]. The material is seen to collapse at around 11.7-GPa compressive stress, in agreement with experimental results in Ref. 17. (c) Plot of the S_{33} compliance coefficient of Si under [001] uniaxial stress. The gradual softening along *Z* leads to the collapse of Si under 11.7-GPa [001] compressive stress. The last two points shown correspond to applied stresses of -11.608 and -11.614 GPa. The corresponding compliances are 0.13 and 0.59 GPa^{-1}. At -11.7 GPa the material has collapsed into the well-known β-tin structure.

The way of generating the strains developed in Sec. II above and in Table I may not be fully optimal, but this point is perhaps not as important as it would have been a few years

TABLE IX. Be elasticity computed under a variety of conditions.

Engine	Energy/stress	LDA/PAW or GGA/ultrasoft	Used		C_{11}	C_{12}	C_{13}	C_{33}	C_{44}	Refined	
			a	c			(GPa)			a	c
VASP	stress	GGA/PAW	2.2826	3.5836	290	23	12	364	162	2.2639	3.5663
VASP	stress	LDA/ultrasoft	2.2826	3.5836	273	15	32	348	158	2.2193	3.5130
VASP	stress	GGA/PAW	2.2639	3.5663	307	29	12	377	164		
VASP	stress	LDA/ultrasoft	2.2193	3.5130	334	39	9	412	173		
VASP	stress	GGA/PAW	2.1851	3.4710	390	66	27	478	189		
VASP	stress	LDA/ultrasoft	2.1851	3.4710	365	54	16	456	185		
ORESTES	energy	LDA	2.1851	3.4710	336	81	21	443	181	2.1851	3.4710
Experiment[a] (0 K extrapolation)					299	27	11	342	166	2.2826	3.5836

[a]Reference 40.

ago, due to a continued drastic decrease in computing costs. It has already been shown by Ref. 9 that elastic data for a cubic material can be extracted from just two simulations with respective strains zero and $[e_1+e_6]$. In that case, the first simulation has cubic symmetry and the second one has monoclinic symmetry. In Table I, we propose the pair $[e1]$, which is tetragonal and $[e_4+e_5+e_6]$, which is rhombohedral. Other schemes are possible, like zero and $[e_1+e_4]$, which is orthorhombic. We do not think that there exists a scheme that is superior for all structures with a same crystal system, or even with a same point group. Occupation of Wyckoff sites is structure dependent. The best scheme is then structure dependent because it should preserve as much of the Wyckoff site symmetry as possible. For some cubic structures, it may be more economical to use a rhombohedral distortion, while for others, it may be more economical to use an orthorhombic distortion.

A. Triclinic example: kyanite

Comparison of our refined elastic coefficients with those calculated by Winkler *et al.*,[18] also shown in Table III, indicates good agreement of the refinement parameters, with the possible exception of coefficient C_{13} that they calculate as 46(1), while we get 70(2) GPa. The smaller differences between the other compressive coefficients C_{11}, C_{12}, C_{22}, C_{23}, and C_{33} can probably be ascribed on one hand to their use of the CASTEP quantum engine, while we used VASP, and on the other hand to slight differences in the methodology. For example, we used the x-ray cell data while they relaxed theirs. Our relaxed cell data, which result from the initial stress and the refined compliance coefficients in our calculations ($a=7.112$, $b=7.848$, $c=5.566$ Å, and $\alpha=90.17°$, $\beta=101.09°$, $\gamma=105.96°$) are not very different from the experimental cell data we used in the calculations (7.126, 7.852, 5.572, 89.99, 101.10, 106.00), nor from the values optimized by Winkler *et al.*[18] (7.075, 7.779, 5.523, 89.74, 101.16, 106.04). Nevertheless, the differences in cell data could account for at least part of the differences in the elastic coefficients.

The mixed compression/shear coefficients, in other words, the coefficients with one index smaller than 4 and the other larger than 3, are roughly in statistical agreement between the two studies. It should be noted that all such coefficients that are not calculated to be zero by one study or the other are also in agreement for the sign. The importance of this remark is that, contrary to the compressive or shear coefficients, the sign of those coefficients would reverse upon reversal of one of the conventions for either tensile or shear strain. This sign agreement of the coefficients confirms that the conventions used for input preparation, for *ab initio* computation, and for analysis in Ref. 18 are identical or equivalent to those we use here. As the two software packages are independent, this fit of magnitudes and signs is a very encouraging indication of the generally high quality of current cutting-edge quantum and analysis software.

The numbers in Table II may help towards appreciation of the improvement brought by least squares with respect to a simple-minded analysis of the raw numbers. First, the existence of computational noise is obvious in all observations: none of the 78 ''observed'' stress components ends up being numerically equal to its recalculated value. In particular, some of the stress components refined for no applied strain differ significantly from their ''observed'' counterparts. This invites to caution towards simplifying assumptions, like considering that stress data coming out of cell relaxation can be equated with zero or directly subtracted from similar stress data derived after application of strain. Even if the program produced a zero value for stress after relaxation, such a value would be on the same footing as any other value because it comes from the same calculation. Even that zero value should then be included in the least-squares adjustment.

It might be correctly argued that better fits with the experiment have been obtained in other papers, or that linear fits of a given stress component for more strain magnitudes could also lead to better values than ours, e.g., by spotting and then neglecting outlying observations. This is of course true. It is also true that, if reanalyzed through our least-squares implementation, the corresponding stress values would lead to even better elastic numbers through processing of the additional, or intrinsically better, stress data, or by downweighting the observations leading to anomalously large discrepancies. The now classical works of Gauss (in 1821, 1823, 1826) show that a weighted least-squares refine-

ment gives statistically the best results that can be extracted from data with known standard error. This is because least squares does not focus on a subset of the data to extract one variable at a time, a procedure that can lead to error propagation, but rather considers all the variables and all the data at the same time.

It should be noted that since kyanite is a problem with 32 atoms per primitive cell, its processing in 8 days on a Pentium 4 required making decisions balancing execution time vs precision of stress data, for example, for the *k* mesh. However, this borderline precision is precisely what makes it an interesting example to expose the trade-offs performed by the least-squares procedure in the extraction of the best possible elastic coefficients and initial stress, given the raw stress data.

B. No pressure applied

The numbers reported in Tables IV–VI are noticeably better than those obtained previously with the energy-based approach.[12] In fact this improvement is probably due to a combination of the use here of VASP with the generalized gradient approximation (GGA), the recent projector augmented wave (PAW) potentials,[21] and the present analysis method, or to a possible intrinsic superiority of stress-based methods as previously pointed out in Ref. 3. The numbers in Ref. 12 were based on the use of the ORESTES engine[23] with the local-density approximation (LDA). The present numbers were obtained with the GGA. We have not performed an exhaustive series of tests separating unambiguously the influence of the various factors because this would require a separate paper, but we are confident that they all contribute one way or another to the resulting stiffness values. Nevertheless, we interpret in Sec. VI F the limited Be data in Table IX in terms of a drastic influence of the cell data used, and a modest influence of the approximation, potential, analysis method, or quantum engine used. The large overestimation of initial stress at x-ray cell data for Be and LDA then causes an underestimation of the relaxed cell size, which ripples into increased elastic coefficients. We trust this analysis on Be to be of more general applicability, and to help in the later decomposition of the smaller effects by other factors.

As fewer simulations are required with the stress-strain approach to reach the same degree of data redundancy because of the six observations per simulation vs one for the energy-based approach, that same redundancy can then be reached in only a fraction of the computing time required for the energy-based approach. This, and the algebraically simpler extension to strained materials, may be the bottom line for superiority of the stress-based approach. Our energy-based approach[12] too can be extended to strained materials with limited effort, but we have no plans to undertake this in the near future.

One item probably worth noting is the sign of the C_{14} stiffness coefficient for α-Al_2O_3, corundum. This sign, which has been reported to be experimentally positive in early work, has been unanimously reported to be experimentally negative since the authoritative and thorough work of Wachtman, Jr., Tefft, Lam, and Stinchfield[33] in 1960. We have now computed this coefficient to be positive by two different methods. We note the negative value of C_{14} calculated by Duan, Karki, and Wentzcovitch,[34] but also the fact that they use rhombohedral axes rather than hexagonal axes for their description of the structure of corundum. In view of the general agreement between the calculated and observed stiffness values except for the sign of C_{14} for corundum, and the match of mixed compression-shear coefficients in the triclinic case in Sec. V A and VI A above, we intend to perform more work in an attempt to clarify this apparent discrepancy.

C. Hydrostatic pressure applied

As can be seen in the results summarized in Table VII, the stiffness coefficients calculated here are within 5% of the experimental values at zero pressure. It is well known that the experiment usually gives stiffness values that are reproducible to about 1%, and probably even better for MgO. Those experimental numbers are accordingly more reliable than the results of our calculations. Nevertheless, the *ab initio* numbers are sufficiently accurate to have been of technological interest in the absence of measured values.

In contrast, our calculated values for the first derivatives turn out to be bracketed by the values printed by the three quoted experimental studies. This is an encouraging sign for their reliability with respect to the experimental first-derivative data.

The considerable spread of values for the second derivative of experimental elastic coefficients suggests that it might be premature to perform comparisons about this point. The rough agreement between the values calculated in the present study and the *ab initio* values reported in Ref. 9 is an encouraging sign. It is not impossible that current *ab initio* methods do in fact lead to better values of the second derivative than those obtained from state-of-the-art diamond-anvil experiments. There is of course no way to be sure of this aspect in the absence of better experimental data.

D. General strain applied

Figure 3 shows the elastic behavior of Ti_4As_3 under [001] uniaxial compressive strain. Partial derivatives of the stiffness coefficients with respect to the varied strain component (or combination of strain components for a more general strain than [001] uniaxial compression) are extracted in a straightforward way as the coefficient of the linear term in a polynomial fit to the curve of the corresponding coefficient vs strain. They are $\partial C_{11}/\partial e_3 = -661$, $\partial C_{12}/\partial e_3 = 81$, $\partial C_{13}/\partial e_3 = -471$, $\partial C_{33}/\partial e_3 = -2241$, $\partial C_{44}/\partial e_3 = -390$, and $\partial C_{66}/\partial e_3 = -181$ GPa.

The corresponding numbers probably have only modest current technological value because there is no current indication that Ti_4As_3 is about to become a ''hot'' material tomorrow. We picked this material at random. However, the numbers in Sec. V D and the above numbers expose clearly the quantum jump in capabilities brought about by linking the CRYSTMET and ICSD crystal structure databases and the automated tools made possible by our present symmetry-general least-squares approaches. Those numbers were produced in straightforward point-and-click fashion on a mate-

rial for which only the structure type was known. Experience that we have gained so far on probably close to 150 elements and compounds now makes us extremely confident that the numbers we show in Secs. V D and VI D are correct. Those numbers comprise the x fractional coordinate of Ti, which we predict to be 0.107 Å away from the center of the fixed-shape As coordination polyhedron, with a shape midway between a trigonal prism and an octahedron (=trigonal antiprism) at 0 K. They also comprise the zero-pressure single-crystal elastic coefficients, and Young's, shear, and bulk moduli for the polycrystalline material. They include the speed of sound for longitudinal and transverse waves and the Debye temperature. They include partial derivatives of stiffness coefficients with respect to any strain component as shown above. Hydrostatic compression curves like we showed for MgO in Sec. VI C, with pressure derivatives, for example, as well as general stressing as shown in Sec. VI E, all become feasible with a few mouse clicks and keystrokes by a moderately experienced user. Of course, the computing power has to be adapted to the pure-phase material selected. In the present example on Ti_4As_3, we used one personal computer (PC) for three days. We feel that this feasibility is a sign of things to come for computational materials science, with more properties to be harnessed, one at a time, but across structure databases.

E. Application of general stress leading to a phase transformation

One may wonder whether this approach might not be optimal in terms of the computing effort. We do not think so because, provided the stress step is chosen to be sufficiently small, only one compliance calculation is to be performed at each step. We in fact performed a second calculation at the final configuration for each step, but derived from it little more than a corroboration of the two facts that (i) compliance was not significantly different and (ii) the calculated stress at the final configuration was indeed quite accurately the desired stress.

The above 2-GPa step only held far from a phase transformation. Below -10 GPa, we had to decrease the step down to 0.5 GPa, and then to 0.1 GPa below -11.5 GPa. Around -11.7 GPa, the S_{33} term becomes anomalous, thus putting an end to this straightforward stepping process. Figs. 4(a) and 4(b), respectively, report the compressive and shear stiffness coefficients for Si. Although large changes are seen on stiffness when applied stress approaches -11.7 GPa, they fail to translate the sudden implosion of the material graphically depicted in Fig. 4(c). This is in agreement with Ref. 17 that reports experimentally a phase change at 12.0 GPa under a [001] uniaxial load. The collapse of the material leads to the well-known β-tin structure type.

F. LDA vs GGA and energy strain vs stress strain on the case of beryllium

The data in Table IX comprise three groups of two or three simulations each. The first group corresponds to stress-strain calculations with VASP using the x-ray experimental cell data, the two approximations, GGA with PAW potentials, and LDA with ultrasoft potentials. The refined elastic data agree reasonably well between themselves and with the experimental data. The notable difference is in the relaxed cell data produced by the two elastic calculations, with GGA/PAW producing a much better cell than LDA/ultrasoft.

The second group of simulations corresponds to the same pair of conditions, but with the relaxed cell data that each approximation refined in the first group. We start seeing notable differences here, with the GGA/PAW results remaining more or less consistent with the experimental values. For the LDA/ultrasoft combination, the elastic coefficients remain compatible with the experimental data, but the values of the three independent diagonal coefficients jump up in this case.

The third group of calculations uses the cell data refined by the energy-based approach with the ORESTES quantum engine and nonultrasoft potentials. The diagonal coefficients jump up for both approximations this time. The elastic coefficients extracted for the same cell data by the three different combinations of approximations, potentials, strain schemes, normal equations, and quantities refined are strikingly similar.

After having dissociated in the above way the separate roles played by the various approximations and cell size, we turn to finding out why the relaxed cell data is so different between GGA/PAW and LDA/ultrasoft. In elastic terms, the cell change is calculable as $\mathbf{E}=-\mathbf{S}\boldsymbol{\Sigma}$, where $\mathbf{E}$ is the strain transforming the old cell into the relaxed cell, $\mathbf{S}$ is the elastic compliance, and $\boldsymbol{\Sigma}$ is the residual stress calculated *ab initio* for the old cell. As the two sets of elastic coefficients for GGA and LDA are quite similar, the larger cell change with LDA is then necessarily due to larger stresses calculated with the x-ray cell data. In fact, the refined initial stress (Σ_1, Σ_3) at the x-ray cell data is (2.56, 0.50) GPa for the GGA/PAW combination and (8.06, 5.24) GPa with LDA/ultrasoft, confirming the above reasoning.

We therefore ascribe the generally accepted superiority of GGA over LDA (Refs. 35–38) not to any superiority in the calculation of stress change or energy change, but to a better evaluation of stress and energy itself. In agreement with our colleagues who are closely associated with quantum software development (see Acknowledgments section), we do not think that there could be any difference between the energy- and stress-based approaches for the extraction of the elastic coefficients other than those caused by the different noise in stress or energy numbers coming out of the simulations for different selections of strain.

VII. SUMMARY AND CONCLUSIONS

We have developed and implemented above a symmetry-general least-squares method for the extraction of elastic coefficients of strained materials from *ab initio* calculations of stress. Implementation differences with an energy-based approach that we published earlier[12] are considerable, requiring, for example, different sets of efficient strains and a different strategy for the least-squares refinement of a different list of variables. However, both methods share the increased precision brought about by the least-squares procedure as well as the generality brought about by the streamlined treat-

ment of the normal equations for all crystal symmetries.

As the stress-strain equations constitute a 27×27 linear system, and therefore an algebraically simple case, a number of applications not readily tractable with the algebraically more complex energy-based approach becomes straightforward. We have detailed calculations for kyanite, a 32-atom triclinic compound, and for a selection of materials with a range of symmetries at zero pressure. We include examples of application to the elastic behavior of materials under hydrostatic pressure on MgO, under general strain on Ti_4As_3, and under general stress on Si. The MgO case leads to good agreement with experimental stiffness, including its first and second pressure derivatives. We report curves of *ab initio* elastic coefficients corresponding to [001] uniaxial straining of Ti_4As_3, a material known only from its cell- and structure-type data, and for which, to our best knowledge, no other experimental data is apparently available, not even a structure refinement. The Si case of uniaxial stressing along [001] shows the evolution of elastic behavior that ends in the collapse of the material at -11.7 GPa, compared with -12 GPa experimentally.

We find the case of beryllium to be quite sensitive to cell data. On that sensitive case, we find that the differences in the values of the refined elastic coefficients between the LDA and GGA approximations, as well as between energy- and stress-based approaches, are minimal if the same cell data is used. This remains true for different implementations in *ab initio* packages based on different pseudopotentials. However, we find the GGA evaluation of relaxed cell data to be consistently closer to observed x-ray cell data than that from LDA. All this points to a better evaluation of stress and energy, but not necessarily to changes in stress and energy, by GGA when compared with LDA. The use of the present method is of course limited to *ab initio* engines that output stress data. Those are less widespread than the total-energy engines.

It should be stressed that it is the symmetry generality of the least-squares approach detailed here that made it possible to produce a robust user interface. This interface goes all the way from crystal structure databases, through transparent preparation of the necessary quantum tasks, up to analysis of *ab initio* results into elastic coefficients. The printout includes derived quantities like Young's modulus, Debye temperature, and a spectrum of thermomechanical properties for the polycrystalline material, all derivable from stiffness. This interface enables even relatively inexperienced users to produce physically relevant results, like those we report above and more, in straightforward point-and-click fashion. The case of Ti_4As_3 demonstrates the current possibility of mining crystal structure databases with *ab initio* software for technological properties. This may be a sign of things to come for computational materials science.

All the above computations were performed using MEDEA (Ref. 15) and VASP (Ref. 16) running on several 1.4-GHz Pentium 4 or equivalent PC's, exploited under various versions of the Windows operating system. Computation costs were accordingly quite modest.

ACKNOWLEDGMENTS

We are very grateful to Dr. Georg Kresse from Vienna University for permission to use a pre-release version of the PAW potentials. We acknowledge numerous useful discussions with Dr. John Rodgers from Toth Information Systems, Inc. (Ottawa, Canada) and with Drs. Erich Wimmer, John Harris, Alex Mavromaras, Jürgen Sticht, and Walter Wolf from Materials Design SARL (Le Mans, France).

*Email address: yvon.le_page@nrc.ca

†Email address: psaxe@MaterialsDesign.com

[1] O. H. Nielsen and R. M. Martin, Phys. Rev. Lett. **50**, 697 (1983).

[2] S. Wei, D. C. Allan, and J. W. Wilkins, Phys. Rev. B **46**, 12 411 (1992).

[3] R. M. Wentzcovitch, B. B. Karki, S. Karato, and C. R. S. Da Silva, Phys. Earth Planet. Inter. **164**, 371 (1998).

[4] S. G. Shen, J. Phys.: Condens. Matter **6**, 8733 (1994).

[5] G. De Sandre, L. Colombo, and C. Bottani, Phys. Rev. B **54**, 11 857 (1996).

[6] W. Duan, R. M. Wentzcovitch, and K. T. Thomson, Phys. Rev. B **57**, 10 363 (1998).

[7] R. Stadler, W. Wolf, R. Podloucki, G. Kresse, K. Furthmller, and J. Hafner, Phys. Rev. B **54**, 1729 (1996).

[8] R. M. Wentzcovitch, N. L. Ross, and G. D. Price, Phys. Earth Planet. Inter. **90**, 101 (1995).

[9] B. B. Karki, L. Stixrude, S. J. Clark, M. C. Warren, G. J. Ackland, and J. Crain, Am. Mineral. **82**, 51 (1997).

[10] C. da Silva, L. Stixrude, and R. M. Wentzcovitch, Geophys. Res. Lett. **24**, 1963 (1997).

[11] B. Kiefer, L. Stixrude, and R. M. Wentzcovitch, Geophys. Res. Lett. **22**, 2841 (1997).

[12] Y. Le Page and P. W. Saxe, Phys. Rev. B **63**, 174103 (2001).

[13] J. R. Rodgers and G. H. Wood, in *Crystallographic Databases, The International Union of Crystallography* (International Union of Crystallography, Chester, UK, 1987), pp. 96–106; http://www.TothCanada.com/

[14] F. H. Allen, Acta Crystallogr., Sect. A: Found Crystallogr. **A54**, 758 (1998); H. Behrens, *XVIIIth Congress and General Assembly of the International Union of Crystallography, Glasgow*, Abstract No. C07.ID.001 (International Union of Crystallography, Chester, UK, 1999).

[15] http://www.MaterialsDesign.com/

[16] G. Kresse and J. Hafner, Phys. Rev. B **48**, 13 115 (1993); Phys. Rev. B **49**, 14 251 (1994); G. Kresse, Ph.D. thesis, Technische Universität Wien, 1993.

[17] M. C. Gupta and A. L. Ruoff, J. Appl. Phys. **51**, 1072 (1980).

[18] B. Winkler, M. Hytha, M. C. Warren, V. Milman, J. D. Gale, and J. Schreuer, Z. Kristallogr. **216**, 67 (2001).

[19] J. K. Winter and S. Ghose, Am. Mineral. **64**, 573 (1979).

[20] J. G. Brainerd, A. G. Jensen, L. G. Cumming, R. R. Batcher, S. G. Begun, H. S. Black, G. M. Grown, C. R. Burrows, H. Busignies, W. G. Cady, P. S. Carter, A. B. Chamberlain, D. Chambers, E. J. Content, J. W. Forrester, R. A. Hackbusch, L. R. Hafstad, J. V. L. Hofgan, J. E. Keister, E. A. Laport, W. Mason, J. F. McDonald, L. S. Nergaard, A. F. Pomeroy, G. Rappaport, E. S. Seeley, R. F. Shea, J. R. Steen, W. N. Tuttle, L. C. Van Atta, K. S. Van Dyke, D. E. Watts, L. E. Whittemore, R. A. Sykes, C. F. Baldwin, W. L.

Bond, J. K. Clapp, C. Frondel, H. Jaffe, W. P. Mason, P. L. Smith, and J. M. Wolfskill, Proc. IRE **37**, 1378 (1949).
[21] G. Kresse and J. Joubert, Phys. Rev. B **59**, 1758 (1999); P. E. Blöchl, *ibid.* **50**, 17 953 (1994).
[22] H. J. Monkhorst and J. D. Pack, Phys. Rev. B **13**, 5188 (1976).
[23] M. Methfessel and M. van Schilfgaarde, Phys. Rev. B **48**, 4937 (1993).
[24] A. Yoneda, J. Phys. Earth **38**, 19 (1990).
[25] S. V. Sinogeikin and J. D. Bass, Phys. Earth Planet. Inter. **120**, 43 (2000).
[26] C. S. Zha, H-K. Mao, and R. J. Hemley, Proc. Natl. Acad. Sci. U.S.A. **97**, 13 494 (2000).
[27] T. H. Duffy and T. J. Ahrens, J. Geophys. Res., [Space Phys.] **100**, 529 (1995).
[28] H. K. Mao and P. M. Bell, J. Geophys. Res., [Space Phys.] **84**, 4533 (1979).
[29] E. A. Perez-Albuerne and H. G. Drickamer, J. Chem. Phys. **43**, 1381 (1965).
[30] J. S. Weaver, T. Takahashi, and W. A. Bassett, NBS Spec. Publ. **326**, 189 (1971).
[31] R. Berger, Acta Chem. Scand., Ser. A **31**, 514 (1977).
[32] C. Kittel, *Introduction to Solid State Physics*, 7th ed. (Wiley, New York, 1996).
[33] J. B. Wachtman, Jr., W. E. Tefft, D. G. Lam, and R. P. Stinchfield, J. Res. Natl. Bur. Stand., Sect. A **64**, 213 (1960).
[34] W. Duan, B. B. Karki, and R. M. Wentzcovitch, Am. Mineral. **84**, 1961 (1999).
[35] T. C. Leung, C. T. Chan, and B. N. Harmon, Phys. Rev. B **44**, 2923 (1991).
[36] B. Hammer, K. W. Jacobsen, and J. K. Norskov, Phys. Rev. Lett. **70**, 3971 (1993).
[37] D. R. Hamann, Phys. Rev. Lett. **76**, 660 (1996).
[38] J. Goniakowski, J. M. Holender, L. N. Kantorovitch, M. J. Gillan, and J. A. White, Phys. Rev. B **53**, 957 (1996).
[39] *Single Crystal Elastic Constants and Calculated Elastic Properties: A Handbook*, edited by Gene Simmons and Herbert Wang (MIT Cambridge, MA, 1971); *Elastic, Piezoelectric, Pyroelectric, Piezooptic, Electrooptic Constants, and Nonlinear Dielectric Susceptibility of Crystals*, Landolt-Börnstein, New Series, Group III, Vol. 11, edited by K.-H. Hellwege and A. M. Hellwege (Springer-Verlag, Berlin, 1979).
[40] J. F. Smith and C. L. Arbogast, J. Appl. Phys. **31**, 99 (1960).